Journal of Engineering Science and Technology
Vol. 14, No. 1 (2019) 305 - 320

ELECTRODYNAMIC CHARACTERISTICS OF WIRE DIPOLE ANTENNAS BASED ON FRACTAL CURVES

ZEYNULLA ZH. ZHANABAEV[1], BEIBIT A. KARIBAYEV[1,*], AKMARAL K. IMANBAYEVA[2], TIMUR A. NAMAZBAYEV[2], SAYAT N. AKHTANOV[1]

[1]Department of Physics and Technology, al-Farabi Kazakh National University, No. 71 al-Farabi, 050040, Almaty, Kazakhstan
[2]Institute of Experimental and Theoretical Physics, Almaty, Kazakhstan
*Corresponding Author: beibitkaribaev7@gmail.com

Abstract

This article presents wire dipole antennas (d = 1 mm, length L_0 = 14.5 cm) based on prefractals n=1, 2, 3 of the original anisotropic geometric fractal. An analytic description of this fractal is proposed through the Heaviside function. The resonant frequencies of fractal antennas are determined using the scaling factors γ of fractals under consideration. The radiation patterns at the resonant frequencies and frequency-dependent characteristics, such as S_{11}, VSWR, and input impedance in the UHF band, were investigated using theoretical and experimental methods. The characteristics of fractal antennas with triangular, isotropic and anisotropic structures are compared. It is shown that the proposed antenna model has advantages over the width of the radiation pattern, the power spectrum, and the technological characteristics of manufacturing and operation.

Keywords: Anisotropic fractal, Impedance, Prefractal, Radiation pattern, Return losses.

1. Introduction

Antennas are an important element of any wireless transmitting and receiving devices, the type and design of which strongly affect the quality of transmission and reception of information. Nowadays, most of the wireless technologies operate on high-frequency bands. Mobile devices and other transceivers designed for various wireless technologies require appropriate multi-band, in some cases ultra-wideband antennas. The advantage of multi-band antennas is that they can be used simultaneously for different wireless networks, such as GSM, Bluetooth, Wi-Fi and WiMAX applications. For this reason, the development and modification of antennas with multi-range properties is an urgent task for researchers. Recently, some work devoted to the study of the antennas properties of various types has been performed [1-6]. Euclidean geometry underlies these antennas and their prototypes.

In recent years, precise attention has been paid to fractal antennas [7-16]. The self-similarity of the structure allows such antennas to resonate on several frequency bands. Detailed studies were carried out in [9]. In [9], a compact ring fractal monopole with the best impedance characteristics for devices of local wireless networks (WLAN) was used. In [10], a triangular shaped fractal antenna for ultra-wideband applications is proposed. In [11], a dipole patch antenna was studied by a combination of Sierpinski and Koch fractals with the fourth iteration (K4C4). The authors noted the quasi-directivity of radiation at resonant frequencies in the range 1.5-14.5 GHz, as well as the possibility of using them for mobile wireless telecommunication systems. In a similar paper [12], a microstrip monopole antenna is shown, made from a combination of Koch and Serpinsky fractals for 2G/3G/4G/5G/WLAN technologies and navigation. The use of a fractal structure also helps in solving the problem of miniaturization of transceivers. In [13], dual-band, with an efficiency of more than 82%, compact patch antennas constructed on the basis of three different fractals are arranged. In [14], a modified view of the fractal (dual-reverse-arrow fractal DRAW) is presented, which is 40% smaller than the triangular patch antenna. The use of the second prefractal "square Koch" in the form of a patch antenna dipole for small satellites also confirms the efficiency of fractal antennas in a technological and constructive manner [15]. In [16], V-shaped wire dipole antennas on the Koch fractal are examined and compared, with angles between radiators 60, 90 and 120 degrees. It is shown that antennas of this type are characterized by a multilobed property of the directional pattern.

Thus, fractal antennas have broad applications, and there is a question, which topology of fractals can provide the efficiency of electrodynamic, technological characteristics. Antenna studies based on isotropic (Minkowski type), triangular (Koch type) and another intermediate (between purely isotropic and anisotropic) fractals are known [17]. In the paper [18] Zhanabaev proposed the algorithm for an "anisotropic fractal", in which the deformation (division into parts) of elements occurs only in one direction. The term "anisotropic fractal" is also used in [19], where a porous medium with various possible fractal dimensions in different directions is considered. The fractalization of a continuous medium is considered in only one direction with a specific dimension. From the specifics of topology, the antenna based on this fractal intuitively reveals the possibility of implementing better radiation directivity characteristics, a simpler technology for automating the assembly and opening of antennas, and so on. Therefore, in this paper, the goal is to theoretically, numerically and experimentally study the basic radio-technical characteristics of an anisotropic fractal antenna.

2. The Theory of Resonant Radiation of Fractal Antennas

2.1. Anisotropic fractal and its analytical description

In an anisotropic geometric fractal with an increase in the prefractal number (hierarchical level), the ∏-shaped parts are formed only in one direction, with the side links not deformed (Figs. 1(a), (b) and (c)) [20]. The prefractal dimension $D = ln5/ln3 = 1.4649$ is realized only in one direction. A feature of this fractal is that any of its prefractals can be described analytically with a relatively simple formula:

$$y = \sum_{i=1}^{n}\left(\frac{A}{3^{n-1}}\right)\sum_{k=1}^{3^n}\left((-1)^{k+1}\theta(x-\frac{k}{3^n})\right), k \neq 3s, s = (3^{j-1})_{j=1}^{n} \quad (1)$$

where n is the number of iterations, A is the amplitude of function $y(x)$, $\theta(x)$ is the Heaviside function [21], and k is quantity of Heaviside function. Figure 1(d) shows the anisotropic fractal (AF) for $n = 3$ according to Eq. (1). Elements of other fractals are deformed in different changing directions, which make it difficult to choose the formula of the construction algorithm. Therefore, a geometrically recursive algorithm is usually used. The Eq. (1) allows describing analytically spectral and power characteristics of antennas.

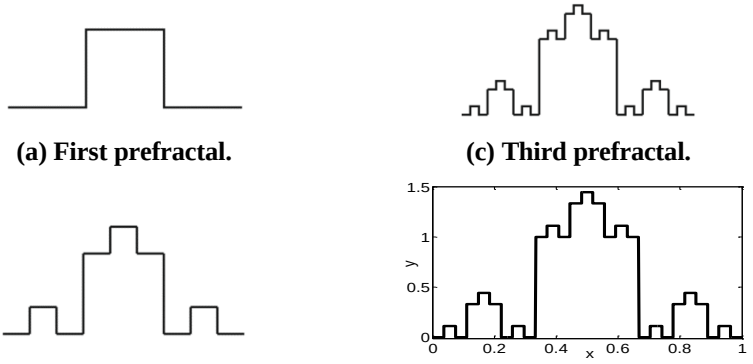

(a) First prefractal. **(c) Third prefractal.**

(b) Second prefractal. **(d) The shape of the fractal curve constructed according to Eq. (1).**

Fig. 1. Structure of the anisotropic fractal.

2.2. Resonant frequency characteristics of fractal antennas

The standard theory of antennas is based on the Maxwell equations for the electromagnetic field, which can be written in differential or integral form. However, fractal antennas having jump like changes in shape cannot be entirely described by continuous variables. Therefore, we will use the methods of fractal geometry.

When one considers the wave propagation only in the x direction, then dot product of kr from the spherical wave formula [22] looks:

$$kr = kx\cos\theta \quad (2)$$

where k is the wave vector, r is the radius vector of the observation point E, θ is the angle between the directions of x and k. From Eq. (2) follows the condition for realizing the maximum $E = E_0$ with respect to time and space:

$$\omega t - kx\cos\theta = 0,\ \omega = k\vartheta = k\vartheta\cos\theta \tag{3}$$

where $\vartheta = \frac{x}{t}$ is the wave propagation velocity, $k = \frac{2\pi}{\lambda}$ is the wave number, and λ is the wavelength. The effective length of the antenna is chosen equal to the wavelength of the received radiation (L=λ). For a fractal structure, L is defined as a fractal measure [23]:

$$L = L_0\delta^{-(D-d)n} = L_0\delta^{-n\gamma},\quad \gamma = D - d \tag{4}$$

where L_0 is the non-fractal (regular) antenna length, δ is the dimensionless measurement scale, D, d are the fractal and topological antenna dimensions, and n is the prefractal number (hierarchical generation).

Substituting Eq. (4) into Eq. (3) we obtain the following:

$$\omega = kv = 2\pi {L_0}^{-1}\delta^{n\gamma}v \tag{5}$$

The ratio of resonance frequencies $(n) = \frac{\omega(n)}{2\pi}$ for prefractals with numbers $n + 1$ and n is:

$$\frac{f_{n+1}}{f_n} = \delta^{\gamma(n+1-n)} = \delta^{\gamma} = \left(\frac{L}{L_0}\right)^{-\frac{1}{n}} \tag{6}$$

In this case the value of f_0 corresponds to the resonant frequency of the half-wave vibrator. Thus, from the known values f_0, δ, and γ, all the antennas resonant frequencies on the fractal are determined. For a given fractal model, δ is the minimum relative strain size, and γ is the difference between fractal and topological dimensions. It also follows from Eq. (6) that the resonant frequency decreases with increasing prefractal number.

2.3. Polarity of antenna radiation

The angle between the x and k directions can be found from Eq. (3) with Eq. (4) taken into account:

$$\theta = 2\pi m \pm arccos(const * \delta^{-n\gamma} f) \tag{7}$$

where m is any integer, f is the antenna resonance frequency (determined by Eq. (6)), $const$ is a constant, which includes slowly varying antenna parameters (the regular length of the antenna L_0 and the wave propagation velocity v) at all prefractals levels. In this case, θ is the angle determining the direction of the maximum radiation relative to the main antenna axis.

2.4. Radiation pattern

The square of the electric field strength, to which the energy of electromagnetic radiation is proportional, can be determined from the equation of motion of an electron under the action of the force "- eE" in the x coordinate [24], also taking into account Eq. (2):

$$\left(\frac{E_x}{E_{0x}}\right)^2 = \delta^{4n\gamma}cos^4\theta \tag{8}$$

It follows from Eqs. (6) and (8) that:

$$\frac{f_{n+1}}{f_n} = \delta^{\frac{\gamma}{4}}. \tag{9}$$

3. Simulation and Measurement of Fractal Antennas Characteristics

3.1. Antenna design

Antennas of other distinctive forms were also investigated by the Koch fractal (KF) and the geometric isotropic Minkowski fractal (IF) to identify the features of the antenna based on AF and compare them [20]. Figure 2 shows the models of antennas under consideration with $n = 2$ as a dipole. KF (with fractal dimension$D = 1.26$, $\delta = 1/3$) is formed by dividing into three equal parts of a single segment and replacing the middle interval by an equilateral triangle without this segment (Fig. 2(b)) [17]. The IF is shown in Fig. 2(c). The generator of this fractal ($D = 1.5$, $\delta = 1/4$) consists of eight links with a length of 1/4. With the growth of the prefractal number, all links are deformed in all directions. The regular length of the all selected samples is L_0 = 14.5 cm, and the distance between radiators is l = 0.5 cm (Fig. 2(a)). Copper with a diameter d = 1 mm (dielectric constant ε = 1.0) was used as a conductive material.

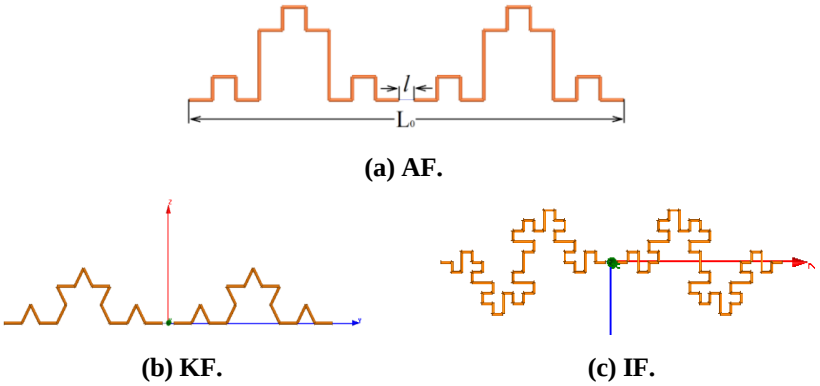

(a) AF.

(b) KF. **(c) IF.**

Fig. 2. Models of wire fractal dipole antennas for *n* = 2 in HFSS.

The software environment HFSS was used, in which the electrodynamic characteristics are calculated by the finite element method to evaluate the antennas performance. The lumped port with a wave impedance of 50 Ohms was installed in designed models. According to the parameters in the frequency range 0.1 - 2.7 GHz (400 points), the frequency-dependent characteristics were determined. They were the following: the reflection coefficient S_{11} of the antenna, *VSWR* between the antenna and the feeder and the input impedance (Z_a), which are described as [25]:

$$S_{11} = \frac{Z_a - Z_0}{Z_a + Z_0}, \quad VSWR = \frac{1+|S_{11}|}{1-|S_{11}|} \tag{10}$$

where $Z_a = R_a + jX_a$ is the input impedance of the load antenna (R_a and X_a are real and imaginary components, respectively), Z_0 is the line impedance, which is

50 Ohm. Three-dimensional (3D) and two-dimensional (2D) radiation patterns were also obtained in the polar coordinate system, and the widths of their main lobes at the -3dB level were determined. The results are given in the next chapter in comparison with measured values.

3.2. Experimental setup

When designing antennas, it becomes necessary to experimentally determine their characteristics in order to verify compliance with their calculated values and, if possible, improve them. The antennas were made in the form of wire dipole radiators. Figure 3 shows the AF antenna prototype in the prefractal with n=2. The parameters necessary for manufacturing the antennas L_0, l, d are selected by the calculated data. The characteristics of the manufactured antennas S_{11}, *VSWR*, input impedance were measured using a vector network analyzer MS46121A. Samples were connected to the VNA via a coaxial cable SYV-50-3, connector SMA male and RF adapter SMA female to type N female (Fig. 4).

Figure 5 shows a block diagram of an experimental setup for the construction of a radiation pattern [26]. The electrical oscillation obtained from the NI PXI-5652 generator is converted into an electromagnetic wave propagating in space using an omnidirectional monopole 2, which is located vertically. The generator has a power of 5 dBm at the resonance frequency. The size of the radiating antenna is chosen correspondingly to the resonance frequency of the receiving fractal antenna 3. The distance from the transmitting antenna to the receiving antenna is 2 m. The signal level in each 5° in the polar coordinate system is measured and fixed using the Agilent N9340B spectrum analyzer. In the special graphical interface 6 radiation pattern is displayed. Figure 6 shows an experimental setup for measuring the power spectrum in the 0.1-2.7 GHz band of a radiating fractal antenna. For generation and reception, a signal generator (where -5 dBm is installed) and a spectrum analyzer, respectively, were used. The measurements were carried out in two modes (Fig. 6(b)). The first, the plane of the fractal antenna XZ was perpendicular to the Y axis, where the receiving horn is located at a distance of 2 m.

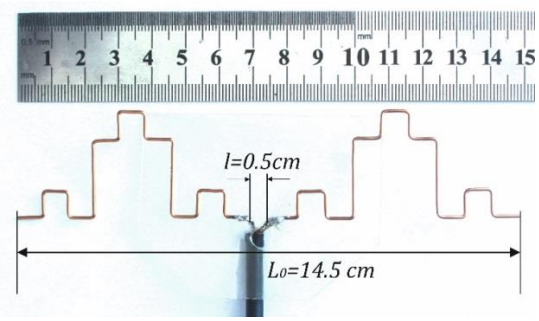

Fig. 3. Manufactured sample of AF antenna with n=2.

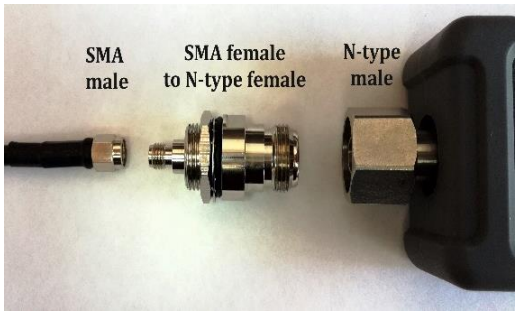

Fig. 4. Used connectors.

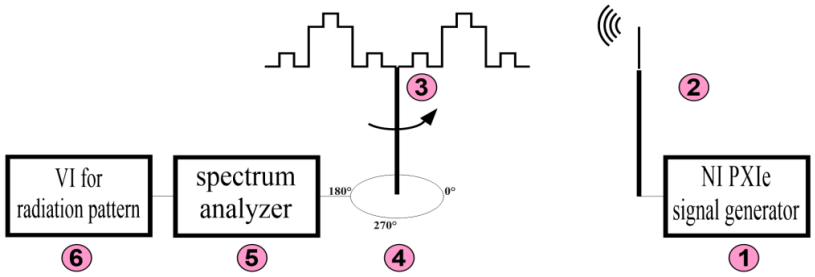

Fig. 5. Block diagram of the experimental setup for the measurement of radiation pattern, 1-RF generator, 2-emitting antenna, 3-fractal receiving antenna, 4-rotary system, 5-spectrum analyzer, 6- graphical interface for constructing radiation pattern.

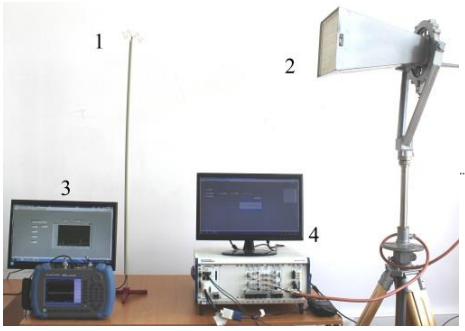

(a) 1-fractal antenna, 2-horn antenna, 3-spectrum analyzer with PC, 4-RF signal generator with PC control.

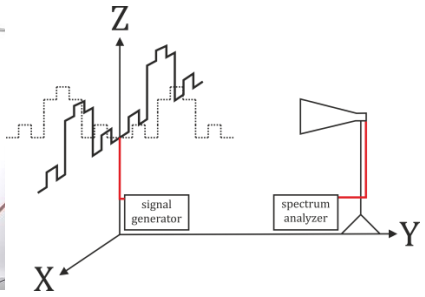

(b) Power spectrum measurement options.

Fig. 6. The hardware-software system of the experimental setup.

The second, the plane of the antenna YZ is parallel to the Y axis. The experimental conditions and the measurement process were the same for all types of antennas. For each antenna were calculated the average values of the power spectrum "P_{avg}".

4. Results of Measurements and Comparisons

4.1. Resonant frequencies

Figure 7 shows simulated (solid lines), measured (dashed lines) return loss of all antennas (S_{11} parameter). It can be seen that all these antennas with fractal structures, as already mentioned above, have several resonance frequencies, in contrast to a half-wave vibrator, which has only one resonance corresponding to the length L_0.

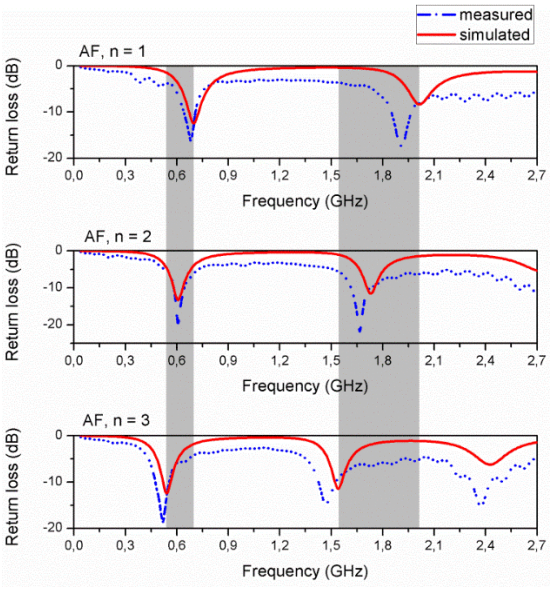

(a) S_{11}- parameters of AF with n=1, 2, 3.

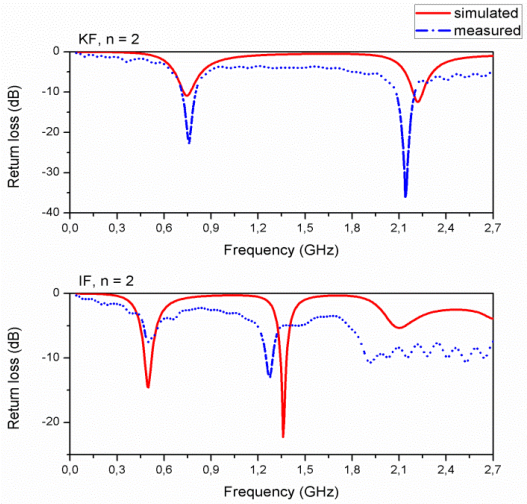

(b) S_{11}- parameters of KF and IF with n=2.

Fig. 7. Dependence of the reflection coefficient on the frequency.

It is also observed that as the iteration number increases, the resonance frequencies shift toward low frequencies (Figs. 7(a) and (b)), where the gray bars indicate the displacements ranges. This offset $f_n > f_{n+1}$ is due to the fact that each successive iteration number will lead to an increase in the fractal length of the antenna L and, accordingly, to a decrease in the resonance frequency according to the Eq. (6). As it follows from the theory, the interval of resonant frequencies in IF (δ=1/4) is smaller than in AF, KF (δ=1/3).

Figure 8 shows the change in resonant frequencies by the prefractal number n. Theoretical dependence according to Eq. (9), the results of simulation in HFSS and direct measurements agree well enough.

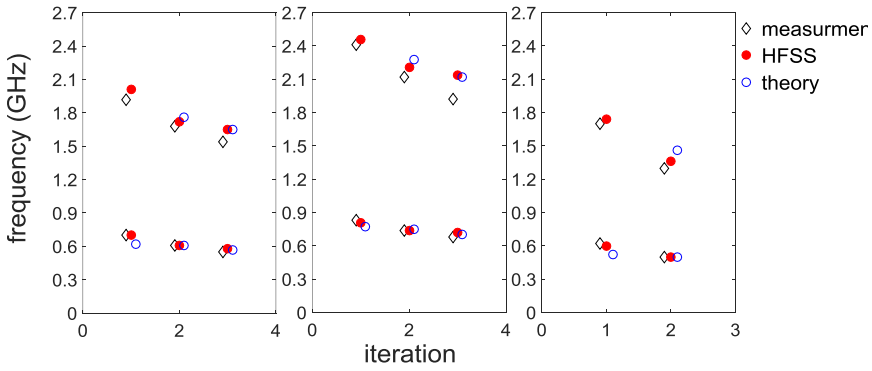

(a) AF. **(b) KF.** **(c) IF.**

Fig. 8. Dependence of resonant frequencies on the *n*-number of the prefractal.

4.2. Polarity of the antenna and the radiation pattern

Figure 9 shows the dependence of the angle between the radiation directions and the antenna's main axis on frequency according to Eq. (7) at $L_0 = 14.5$ cm, n=2.

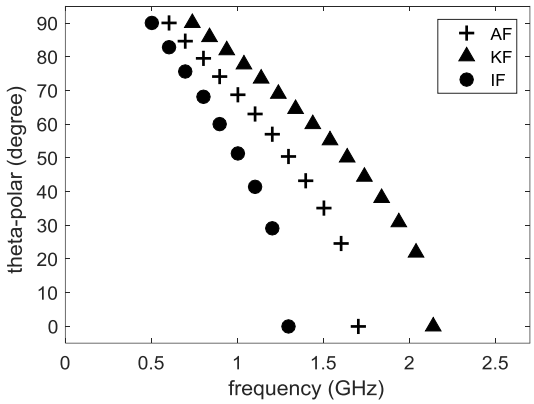

Fig. 9. Change in the direction of maximum radiation by frequency.

It is noticeable that all the considered antennas around their first resonance frequencies $f1$ (0.61 GHz for AF, 0.50 GHz for IF and 0.74 GHz for KF) emit at $\frac{\pi}{2}$

angle to the antenna axis, near the second resonances $f2$ (1.72 GHz for AF, 1.36 GHz for IF) radiation are directed along the main axis, that is, $\theta = 0°$. In the case of KF at 2.21 GHz, the direction of the main lobe (consisting of two narrow lobes) along the antenna axis is also observed. 3D radiation patterns of antennas also show changes in the polarity of the radiation at resonance frequencies (Fig.10).

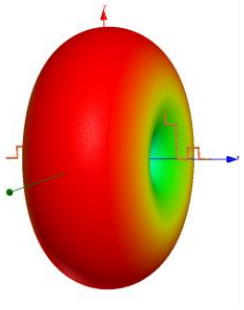

(a) AF at $f1$=0.61 GHz.

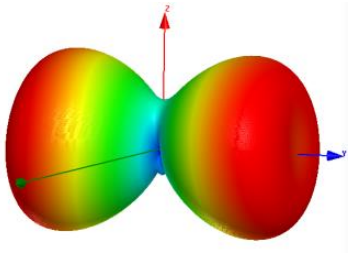

(b) AF at $f2$=1.72 GHz.

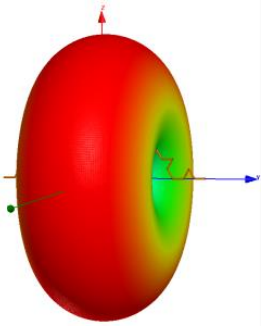

(c) KF at $f1$=0.74 GHz.

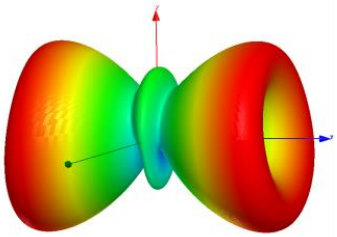

(d) KF at $f1$= 2.22 GHz.

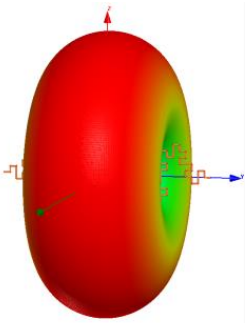

(e) IF at $f1$=0.50 GHz.

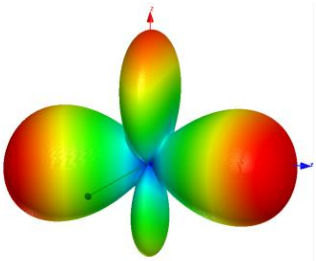

(f) IF at $f2$ = 1.36 GHz.

Fig. 10. Simulated 3D radiation patterns of wire dipole antennas with n = 2 at resonance frequencies $f1$ and $f2$.

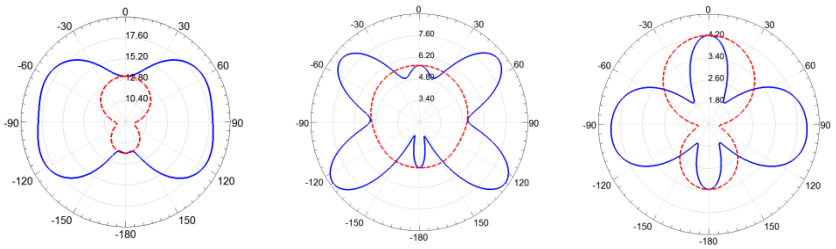

(a) AF. (b) KF. (c) IF.

Fig. 11. Simulated in HFSS 2D radiation patterns of fractal antennas in E (solid) and H (dashed) planes at *f*2 and *n* = 2.

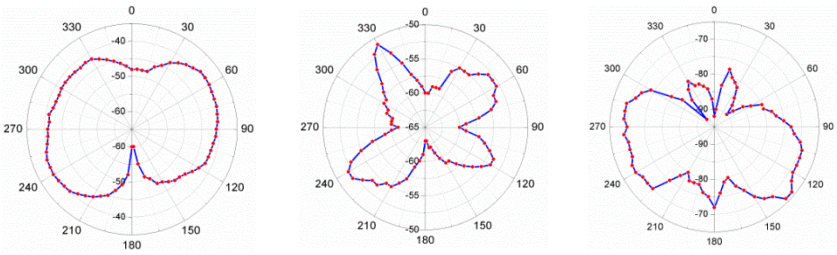

(a) AF. (b) KF. (c) IF.

Fig. 12. Measured 2D radiation patterns of fractal antennas in E plane at *f*2 and *n* = 2.

All the fractal antennas at all levels of the prefractal function at the first resonance frequencies *f*1, as a standard symmetrical half-wave vibrator, emitting the same intensity in directions perpendicular to the antenna axis. Therefore, antenna comparisons were carried out for *f*2. The two-dimensional radiation patterns obtained in the HFSS environment (Fig. 11) correspond to the measured ones (Fig. 12). The antenna of the KF-based antenna differs in that it has a multilobed shape. This is explained as follows: if we consider the antenna shapes AF and IF, then in the fractal structure all the links are located perpendicular to each other at all levels of the prefractal, i.e., the angle θ indicating the vector direction k is defined as $\theta \pm \pi/2$. For FK, we have $\theta \pm \pi/3$, since the internal angle of an equilateral triangle is $\alpha = \pi/3$. These factors will lead to a multidirectional antenna FK in comparison with AF and IF. A further increase in frequency will result in a smooth change in the radiator direction. At frequency *f*2, the radiation pattern of the AF-based antenna sample has two main directed lobes (Figs. 11(a) and 12(a)), whereas KF, IF have a multi-lobe radiation pattern. Table 1 shows the quantitative parameters of the directivity at the second resonance frequency.

Table 1. Characteristics of 2D radiation patterns of antennas.

Type of fractal antenna	No. of iteration	Resonant frequency *f2* (GHz)	Main lobe magnitude (V)	Beam width of main lobe at "-3 dB" (degree)
AF	2	1.72	8.56	123.52
KF	2	2.22	8.86	46.08
IF	2	1.36	4.58	93.85

4.3. VSWR and Impedance

The matching of impedance is an important point in the development of antennas. It follows from Eq. (10) that if $|S_{11}|$=0, then *VSWR* = 1. In practice, reflection is always present and *VSWR* is in the interval [1.1 ÷ +∞]. A value greater than two results in an inconsistency (mismatch) system.

Table 2 below compares the values obtained by simulation and measurements for all types of investigated antennas at resonant frequencies.

Table 3 shows the *VSWR* values of all fractal antennas.

Table 2. Impedance of fractal antennas at resonant frequencies (Ohm).

Type of fractal antenna		No. of iteration					
		1		2		3	
		$f1$	$f2$	$f1$	$f2$	$f1$	$f2$
AF	measurement	66.56	57.62	37.63	49.74	62.24	46.69
IF	measurement	36.27	77.51	26.82	149.55	58.72	25.19
KF	measurement	56.40	59.70	46.80	48.59	51.93	47.12

Table 3. VSWR of fractal antennas at resonant frequencies.

Type of fractal antenna		No. of iteration					
		1		2		3	
		$f1$	$f2$	$f1$	$f2$	$f1$	$f2$
AF	measurement	1.3	1.2	1.4	1.1	1.7	1.1
	simulation	1.6	2.0	1.5	1.7	1.5	1.6
IF	measurement	1.3	1.5	2.0	3.2	-	-
	simulation	1.5	1.2	1.4	1.2	-	-
KF	measurement	1.1	1.3	1.1	1.0	1.2	1.3
	simulation	1.9	2.2	1.8	1.6	1.7	1.4

Thus, concerning investigated AF, the following conclusion can be drawn:

- For all resonant frequencies AF samples have *VSWR* <2 within norm limits.
- Due to the permissible impedance value (Ω = ~50 Ohms), AF antennas do not require special matching elements and circuits with corresponding parameters (as in the experiment), in contrast to the IF antenna (where for n=2, $f2$: Ω > 50 Ohm).

4.4. The average value of the radiation power in frequency

The dependence of root mean square values of P_{rms} on the prefractal number n is given below. The radiation power of the AF antenna is greater than that of the KF and IF antennas for all levels of prefractals when the antenna plane is perpendicular to the Y axis (Fig. 13(a)). Figure 13(b) shows a graph for the case where the position of the antenna plane is parallel to the Y axis. At n=1, the average power P_{rms} of the AF antenna radiation (100 μW) is below the IF antenna power (130 μW). With the exception of this case, for all prefractals (n = 1, 2, 3), the radiation power of the AF antenna is higher than that of the KF and IF antennas.

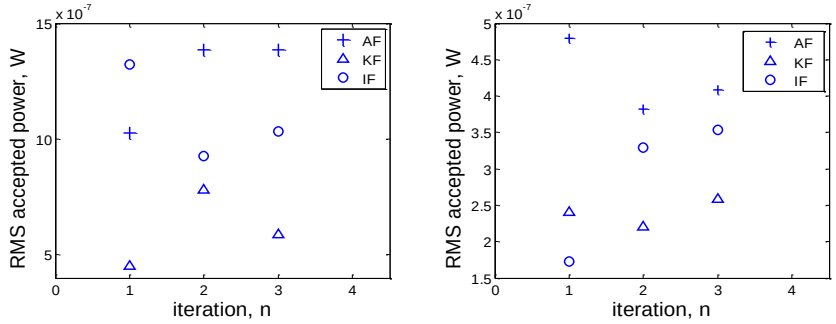

(a) The antenna plane is perpendicular to the wave propagation direction.

(b) The antenna plane of is parallel to the wave propagation direction.

Fig. 13. Experimental mean-square values (RMS) of the power spectrum for AF (+), KF (Δ) and IF (○).

5. Conclusions

This article presented the possibility of creating an antenna based on a new kind of geometric fractal, such as an anisotropic fractal. This structure is described by an analytical formula and has a constant fractal dimension in only one direction, unlike the other known geometric fractals.

The frequency properties and directionality of radiation of three types of wire fractal antennas of AF, KF, IF in a dipole version are theoretically described. Theoretical results are confirmed by numerical simulation in the HFSS medium and by a physical experiment. Antennas based on geometric fractals have a multi-frequency property, unlike standard half-wave vibrators. With the growth of the iteration number, the resonance frequency shifts towards decreasing because of the length growth of the fractal antenna. At resonant frequencies, radiation patterns of fractal antennas differ in the radiation polarity, that is, in the transition from the first $f1$ to the second $f2$ resonant frequency, the radiation direction changes in all antennas under consideration. All studied electromagnetic characteristics are compared for three species, covering anisotropic and isotropic fractal antennas. Complex analysis (theory, simulation and physical experiment) shows that an antenna based on an anisotropic fractal has an advantage (up to 15-20% compared to other fractal antennas) for all characteristics, such as radiation pattern, radiation power, impedance, etc. Antenna on based anisotropic fractal also has technological advantages of manufacturing from the point of view of automatic opening and collection. Therefore, such antennas can find wide applications, for example, for satellites of small size, and also in robotics.

Acknowledgment

This work has been supported by the Ministry of Education and Science of Kazakhstan under grant number AP05132738 "Information entropy technologies of multichannel telecommunication systems and their application". The study was conducted in the laboratory of nonlinear physics of the Institute of Experimental and Theoretical Physics.

Nomenclatures

D	Fractal dimension
d	Wire diameter, mm or Topological dimension
L	Fractal antenna length, cm
L_0	Non-fractal (regular) length of antenna (Fig. 1), cm
l	Gap between the vibrators (Fig. 1), cm
n	Number of iteration
P_{rms}	Root means square value of the power, W
R_a	Real component of impedance
S_{11}	Return losses or reflection coefficient, dB
X_a	Imaginary component of impedance
Z_0	Impedance of the cable (feeder), Ohm
Z_a	Input impedance of the antenna, Ohm

Greek Symbols

$\theta(x)$	Heaviside function
δ	Scale of measurement
γ	Difference of fractal and topological measure (D - d)
θ	Angle of maximum radiation, deg.

Abbreviations

AF	Anisotropic fractal
KF	Koch fractal
IF	Isotropic fractal
VSWR	Volt standing wave ratio

References

1. Arand, B.A.; and Bazrkar, A. (2015). Gain enhancement of a tetra-band square-loop patch antenna using an AMC-PEC substrate and a superstrate. *Wireless Personal Communications*, 84(1), 87-97.
2. Ding, H.Z.; Jiao, Y.C.; and Ni, T. (2015). A compact multiband printed antenna for smart-phone applications. *Microwave and Optical Technology Lett*, 57 (10), 2289-2294.
3. Saha, R.; and Maity, S. (2016). Ameliorate of bandwidth and return loss of rectangular patch antenna using metamaterial structure for RFID technology. *Journal of Engineering Science and Technology*, 9(11), 1249-1262.
4. Bartwal, P.; Gautam, A.K.; Singh, A.K.; Kanaujia, B.K.; and Rambabu, K. (2016). Design of compact multi-band meander-line antenna for global positioning system/wireless local area network/worldwide interoperability for microwave access band applications in laptops/tablets. *IET Microwaves Antennas & Propagation*, 10(15), 1618-1624.
5. Gupta, S.D.; and Srivastava, M.C. (2012). Multilayer microstrip antenna quality factor optimization for bandwidth enhancement. *Journal of Engineering Science and Technology*, 6(7), 756-773.

6. Thomas, K.G.; and Sreenivasan, M. (2010). Compact CPW-fed dual-band antenna. *Electronics Letters*, 46(1), 13-14.
7. Nobrega, C.D.; da Silva, M.R.; Silva, P.H.F.; D'Assuncao, A.G.; and Siqueira, G.L. (2015). Simple, compact, and multiband frequency selective surfaces using dissimilar Sierpinski fractal elements. *International Journal of Antennas and Propagation*, Volume 2015, Article ID 614780, 5 pages.
8. Minervino, D.R.; D'Assuncao, A.G.; and Peixeiro, C. (2016). Mandelbrot fractal microstrip antennas. *Microwave and Optical Technology Letters*, 58(1), 83-86.
9. Ghobadi, C.; Nourinia, J.; Pourahmadazar, J.; and Shirzad, H. (2010). Multiband ring fractal monopole antenna for mobile devices. *IEEE Antennas and Wireless Propagation Letters*, 9, 863-866.
10. Gupta, M.; and Mathur, V. (2016). A new printed fractal right angled isosceles triangular monopole antenna for ultra-wideband applications. *Egyptian Informatics Journal*, 18(1), 39-43.
11. Li, D.; and Mao, J.-F. (2012). Sierpinskized Koch-like sided multifractal dipole antenna. *Progress in Electromagnetics Research*, 130, 207-224.
12. Yu, Z.; Yu J.; Ran, X.; and Zhu, C. (2017). A novel Koch and Sierpinski combined fractal antenna for 2G/3G/4G/5G/WLAN/navigation applications. *Microwave and Optical Technology Letters*, 59(9), 2147-2155.
13. Kakoyiannis, C.G.; Constantinou, P. (2013). Compact, slotted, printed antennas for dual-band communication in future wireless sensor networks. *International Journal of Antennas and Propagation*, Volume 2013, Article ID 873234, 17 pages.
14. Orazi, H.; Soleimani, H. (2015). Miniaturisation of the triangular patch antenna by the novel dual-reverse-arrow fractal. *IET Microwaves, Antennas & Propagation*, 9(7), 627-633.
15. Simon, J.; Alvarez-Flores, J.L.; Villanueva-Maldonado, J.; Castillo-Topete, V.H.; Soriano-Equigua, L.; and Flores-Troncoso, J. (2017). A microstrip second-iteration square Koch dipole antenna for TT&C downlink applications in small satellites. *International Journal of Antennas and Propagation*, 2017, Article ID 4825179, 8.
16. Vinoy, K.J.; Jose, K.A.; and Varadan, V.K. (2003). On the relationship between fractal dimension and the performance of multi-resonant dipole antennas using Koch curves. *IEEE Transactions on Antennas and Propagation*, 51(9), 2296-2303.
17. Mandelbrot, B.B. (1983). *The fractal geometry of nature* (updated and augmented). New York: W.H. Freeman and company.
18. Zhanabaev, Z. (1988). Fractal model of turbulence in the jet. *Proceedings of the SB Academy of Science USSR*, 4, 57-60.
19. Li, J.; and Ostoja-Starzewski, M. (2009). Fractal solids, product measures and fractional wave equations. *Proceedings of the Royal Society A: Mathematical, Physical and Engineering Sciences*, 465, 2521-2536.
20. Zhanabaev, Z.Z.; Karibayev, B.K.; Namazbayev, T.A.; Imanbayeva, A.K.; Temirbayev, A.A.; and Ahtanov, S.N. (2017). Fractal antenna with maximum capture power. *ACM International Conference Proceeding Series. 6th*

International Conference on Telecommunications and Remote Sensing. Delft, Netherlands, 17-20.

21. Kanwal, R.P. (1988). *Generalized functions: theory and technique* (2nd ed.). Boston: Birkhauser.
22. Fitzpatrick, R. (2008). *Maxwell's equations and the principles of electromagnetism.* Jones & Bartlett Publishers.
23. Feder, J. (1988). Fractals. New York: Plenum Press.
24. Rohrlich, F. (2007). *Classical charged particles* (3rd ed.). World scientific.
25. Huang, Y.; and Boyle, K. (2008). *Antennas: from theory to practice* (1st ed.). Singapore: John Wiley and Sons Inc.
26. Karibayev, B.A.; Zhanabaev, Z.Z.; Temirbayev, A.A.; Imanbayeva, A.K.; and Namazbayev, T.A. (2017). Pattern lobes and beam widths of a novel fractal antenna. *Eurasian Physical Technical Journal,* 14(2), 57-60.